Aust. Met. Mag. 47 (1998) 295-308

An overview of the HYSPLIT_4 modelling system for trajectories, dispersion and deposition

Roland R. Draxler
NOAA Air Resources Laboratory, Silver Spring, Maryland, USA
and
G.D. Hess
Bureau of Meteorology Research Centre, Australia

(Manuscript received June 1997; revised January 1998)

The HYSPLIT_4 (HYbrid Single-Particle Lagrangian Integrated Trajectory) model is designed for quick response to atmospheric emergencies, diagnostic case studies, or climatological analyses using previously gridded meteorological data. Calculations may be performed sequentially on multiple meteorological grids, going from fine to coarse resolution and using either archive or forecast data fields. Air concentration calculations associate the mass of the pollutant species with the release of either puffs, particles, or a combination of both. The dispersion rate is calculated from the vertical diffusivity profile, wind shear, and horizontal deformation of the wind field. Air concentrations are calculated at a specific grid-point for puffs and as cell-average concentrations for particles. The model results are evaluated against ACE balloon trajectories, air concentrations from the ANATEX tracer experiment, radiological deposition from the Chernobyl accident, and satellite photographs of the Rabaul volcanic eruption. One common feature of the model results was their sensitivity to the vertical atmospheric structure; trajectories in terms of their height when near ground-level due to the strong gradients of wind speed and direction, air concentrations with respect to the rate of vertical mixing, and deposition as a result of the vertical distribution of the pollutant.

Introduction

Atmospheric dispersion modelling, the use of numerical methods to compute the time history of air pollutant concentrations, is usually divided into two broad categories. Eulerian models, which solve the advection-diffusion equation on a fixed grid, and Lagrangian models, in which the advection and diffusion components are calculated independently. Eulerian methods are typically applied when complex emission scenarios are considered, requiring solutions at all grid-points. Lagrangian methods are typically favoured when single-point-source emissions restrict computations to a few grid-points. Further, Eulerian models generally require emissions to be defined on a scale comparable to the model's computational grid while Lagrangian models can define the emissions at any resolution. These considerations aside, a review of the literature will show that both

Corresponding author address: Roland R. Draxler, 1315 East West Highway, Room 3151, Silver Spring , MD 20910, USA.

methods have been successfully applied to a variety of different scenarios. The intent in this paper is to review the details of a Lagrangian dispersion model (HYSPLIT_4 - HYbrid Single-Particle Lagrangian Integrated Trajectories Version 4) designed to support the Bureau of Meteorology (BoM) in its need to respond to atmospheric emergencies ranging in character from accidental radiological releases to the hazards presented to aircraft operations from volcanic ash eruptions.

The model calculation method is a hybrid between Eulerian and Lagrangian approaches. Advection and diffusion calculations are made in a Lagrangian framework while concentrations are calculated on a fixed grid. The model has evolved over several stages during the last decade and a half. The initial version of the model (Draxler and Taylor 1982) used only rawinsonde observations and the dispersion was assumed to consist of uniform mixing during the daytime and no mixing at night. Dispersion due to wind shear was introduced by splitting up the daytime mixed layer into smaller layers each night. In the next revision (Draxler and Stunder 1988), variable strength mixing was introduced based upon a temporally and spatially varying diffusivity profile. In the last revision (HYSPLIT_3 – Draxler 1990; 1992), the use of rawinsonde data was replaced by gridded meteorological data from either analyses or short-term forecasts from routine numerical weather prediction models. It was shown (Draxler 1991) that these routine products provided calculations that were as accurate as those made using rawinsondes, even when special off-time (0600 and 1800 UTC) soundings were included in the calculations.

Several significant new features have been added to the current version of the model. In particular, the advection algorithms have been updated to include temporal interpolation and although the dispersion of a pollutant can still be calculated by assuming the release of a single puff, the puff can now be defined with either a Gaussian or top-hat horizontal distribution. As in previous versions, a single released puff will expand until its size exceeds the meteorological grid cell spacing, and then it will split into several new smaller puffs. Further, a three-dimensional particle dispersion routine has been added that computes air concentrations from the dispersal of an initial fixed number of particles. The particle approach includes a modification, following Hurley (1994), that combines both puff and particle methods by assuming a puff distribution in the horizontal and particle dispersion in the vertical direction. This hybrid calculation may be started with a single particle. In this way, the greater accuracy of the vertical dispersion parametrisation of the particle model is combined with the advantage of having an expanding number of puffs represent the pollutant distribution as the spatial coverage of the pollutant increases. Perhaps more significantly, all the equations used to compute the strength of the vertical mixing have been revised based upon the more recent literature, and the rate of horizontal dispersion is no longer assumed to be constant but can vary according to the deformation of the wind field. In general only the features of the model that have changed significantly from the previous HYSPLIT version will be discussed in any detail in the following sections, however a complete technical description of the model, including all equations that have been omitted here, can be found in Draxler and Hess (1997).

Trajectories

The basis of any Lagrangian model is that the dispersion is computed following the particle or puff. That is, the advection of a particle is computed independently of the dispersion calculation. The time integrated advection of each particle can be viewed as a simple trajectory which only requires the three-dimensional velocity field.

Meteorological data

Meteorological data for trajectories and dispersion calculations are obtained as output fields from meteorological models. Usually these fields cannot be directly used by HYSPLIT without some pre-processing. Although most meteorological models use some variation of a terrain-following coordinate system, the data fields are usually interpolated to a variety of different vertical coordinate systems prior to output. To maintain a larger degree of flexibility within HYSPLIT's internal structure, i.e. the ability to use different meteorological data sources for input, the profiles of the meteorological data at each horizontal grid point are linearly interpolated to a terrain-following (σ) coordinate system,

$$\sigma = 1 - z/Z_{top} \qquad \ldots 1$$

where all the heights are expressed relative to terrain and where Z_{top} is the top of HYSPLIT's coordinate system. The model is capable of handling meteorological data fields provided on four different vertical coordinate systems: pressure-sigma, absolute-pressure, terrain-sigma (typically used in mesoscale models covering a limited spatial domain), or a hybrid absolute-pressure-sigma coordinate system (ECMWF 1995; which consists of an absolute pressure added to the pressure-sigma level).

The dispersion model's horizontal grid system is always identical to that of the meteorological input data. Three different conformal map projections are supported, Polar Stereographic, Mercator, and Lambert Conformal, using a set of universal mapping transformation routines (Taylor 1997). A simulation may use

several meteorological data files, each on different projections. For instance, a calculation may start on a Lambert Conformal regional grid and then switch to the Polar Stereographic global grid. Gridded fields of meteorological variables are also required at regular temporal intervals which should be constant for each defined grid, i.e. the regional grid may be available at 3 h intervals while the coarser global grid may be available only every 6 h.

At a minimum HYSPLIT requires U, V (the horizontal wind components), T (temperature), Z (height) or P (pressure), and the pressure at the surface, P_0. If wet deposition processes are to be included, then the model also requires the rainfall field. Normally ground-level (≤10 m) winds are available from most meteorological models. In the rare case when these fields are not provided, these winds are estimated using a logarithmic profile for neutral conditions.

In most circumstances the meteorological data will contain a vertical motion field, usually in pressure units, and regardless upon which vertical coordinate system these data are provided, the vertical velocity field is almost always relative to the meteorological model's native terrain-following coordinate system. The trajectory and dispersion model calculations can use these data fields directly because the model's internal coordinate system is terrain following. This is one of the primary reasons why the meteorological data for the dispersion model are always re-mapped internally to a common terrain following vertical coordinate system.

When the vertical motion fields are missing, or perhaps there are some special conditions required for a simulation, HYSPLIT has an option to replace these fields with a vertical velocity calculated based upon an assumption that the pollutant parcel is transported on some other surface. The velocity (W_η) to maintain a parcel on the selected (η) surface is computed from,

$$W\eta = (-\partial\eta/\partial t - u\,\partial\eta/\partial x - v\,\partial\eta/\partial y) / (\partial\eta/\partial z) \qquad ...2$$

given the slope of the surface and its local rate of change. The surfaces, η, may be defined as isobaric (p), isosigma (σ), isopycnic (ρ), or isentropic (θ).

Advection calculation

Once the basic (U,V,W) meteorological data have been processed and interpolated to the internal model grid, trajectories can be computed to test the advection components of the model. The key improvement in the advection calculation over previous versions of the model is that time interpolation of the meteorological fields is directly incorporated into the advection algorithm. The advection of a particle or puff is computed from the average of the three-dimensional velocity vectors for the initial-position $P(t)$ and the first-guess position $P'(t+\Delta t)$. The velocity vectors are linearly interpolated in both space and time. The first guess position is

$$P'(t+\Delta t) = P(t) + V(P,t)\,\Delta t \qquad ...3$$

and the final position is

$$P(t+\Delta t) = P(t) + 0.5\,[V(P,t) + V(P',t+\Delta t)]\,\Delta t \qquad ...4$$

Trajectories are terminated if they exit the model top, but advection continues along the surface if trajectories intersect the ground. The integration time step (Δt) can vary during the simulation. It is computed from the requirement that the advection distance per time-step should be less than 0.75 of the meteorological grid spacing.

The integration method (e.g. Kreyszig 1968) is common and has been used for trajectory analysis (Petterssen 1940) for quite some time. Higher-order integration methods were investigated but as long as the data observations are linearly interpolated from the grid to the integration point, higher-order methods will not yield greater precision.

Trajectory example - ACE

Following a balloon path provides an excellent test of a model's advection calculation (Draxler 1996). A sample trajectory calculation was made for the time and place from which three constant-level balloons were released on 8 December 1995 during the first Aerosol Characterization Experiment (ACE - S.T. Siems, personal communication; Bates et al. (1998)) south of Tasmania. The meteorological data were obtained from NOAA's global AVN model (Peterson and Stackpole, 1989) at an output resolution of 190 km on mandatory pressure surfaces at 12-h intervals, and the BoM global GASP model (Bourke et al. 1995) at an output resolution of 285 km (2.5°) on 19 vertical levels at 12-h intervals. Data from 6-h forecasts from the AVN and GASP models were used in the period between analyses. The balloons were tracked for 24 hours, each released about one hour apart, and each had a slightly more westerly path. The calculated and observed trajectories for the first balloon are shown in Fig. 1, where the calculated trajectories are labelled as 'GASP' and 'NOAA' according to the meteorological data used for the calculation. The trajectory calculation was started from the 0000 UTC balloon position and height (about 200 m AGL - above ground level). Although the calculated tracks are close to the balloon's path, the measured balloon track ends slightly to the west of all the calculations. After 24-h, the observed differences of 10 per cent to 20 per cent of the transport distance are consistent with previous studies (Draxler 1996, 1991) of trajectory accuracy in an inhomogeneous environment. It is seen that the two models produce results that are in close agreement with each

Fig. 1 **ACE balloon path and corresponding calculated trajectories using GASP and NOAA meteorological data for a starting time of 0000 UTC 8 December 1995. Latitude and longitudes are indicated at 2 degree intervals.**

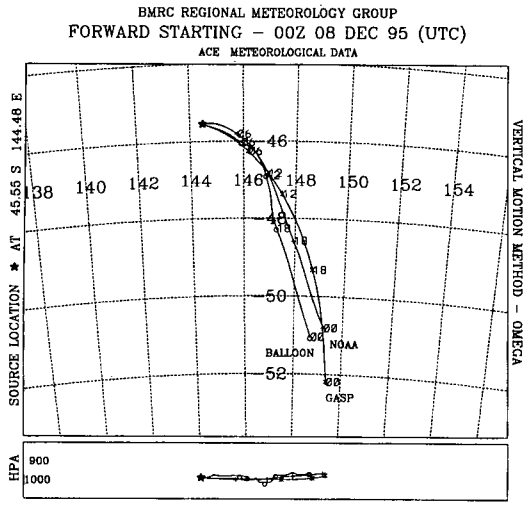

Fig. 2 **Calculated trajectories using NOAA meteorological data starting at four different positions 0.5 degrees about the initial ACE balloon position. Latitude and longitudes are indicated at 2 degree intervals and trajectory positions are marked every 6 h.**

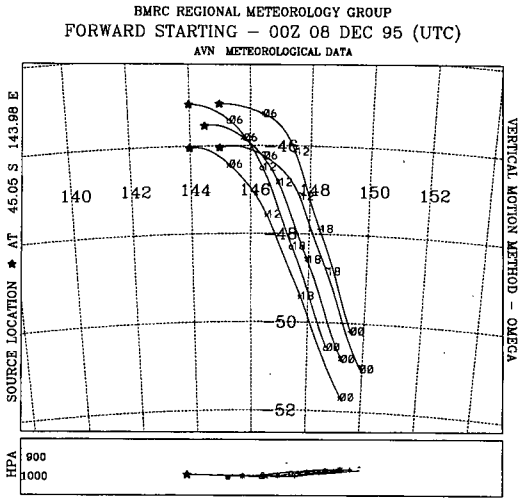

other, although the GASP model exhibits faster winds and its trajectory travels further south on this occasion.

The sensitivity of the calculated trajectory to initial position can be evaluated by starting simultaneous trajectories at different heights and levels. Trajectories started at ±0.5° about the origin measure the homogeneity of the wind field and the results using the AVN meteorological data are shown in Fig. 2. Clearly all the trajectories are parallel to each other and slight errors in horizontal position would have made little difference in any accumulated trajectory error. However when trajectories are started at 3 different heights (10, 200 and 750 m AGL) the resulting differences shown in Fig. 3 are quite substantial. The actual balloon track did not follow a constant altitude and at times travelled much closer to the surface than the 200 m trajectory would indicate and as expected the measured horizontal balloon path falls between the 10 m and 200 m calculated trajectories. This is only a single illustrative case and a more formal evaluation would require many more cases before quantitative conclusions could be drawn from the results. However, due to the larger variations of wind speed and direction near the ground than at higher altitudes, it is clear that proper specification of the atmosphere's vertical structure is essential for the accurate computation of boundary layer pollutant transport.

Fig. 3 **ACE balloon path and calculated trajectories using NOAA meteorological data starting at three different heights, 10 m, 200 m, and 750 m AGL. Latitude and longitudes are indicated at 2 degree intervals, trajectory positions are marked every 6 h, and the balloon heights are indicated at the end of each trajectory in pressure units.**

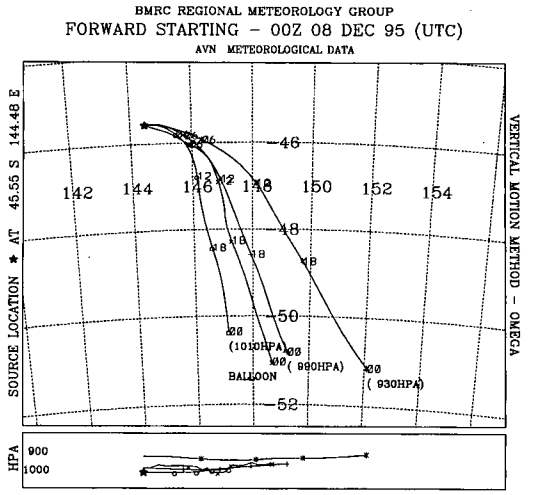

Air concentrations

A Lagrangian model can compute air concentrations through either of two assumptions. In a puff model, the source is simulated by releasing pollutant puffs at regular intervals over the duration of the release. Each puff contains the appropriate fraction of the pollutant mass. The puff is advected according to the trajectory of its centre position while the size of the puff (both horizontally and vertically) expands in time to account for the dispersive nature of a turbulent atmosphere. Air concentrations are then calculated at specific points (or nodes on a grid) by assuming that the concentrations within the puff have a defined spatial distribution. In a Lagrangian particle model, the source can be simulated by releasing many particles over the duration of the release. In addition to the advective motion of each particle, a random component to the motion is added at each step according to the atmospheric turbulence at that time. In this way a cluster of particles released at the same point will expand in space and time simulating the dispersive nature of the atmosphere. Air concentrations are calculated by summing the mass of all the particles in a grid cell. In a homogeneous environment the size of the puff (in terms of its standard deviation) at any particular time should correspond to the second moment of the particle positions.

Although a particle approach can more realistically represent dispersion in an inhomogeneous atmosphere, the puff methods used in HYSPLIT permit the puffs to split into smaller components when they exceed certain dimensions, usually the dimensions of the meteorological grid. In this way, subgrid turbulence processes are modelled by the dispersion parametrisations while grid-scale processes are simulated by the puff splitting process. However, one limitation of puff splitting is that it can generate too many puffs, especially in the vertical direction if the mixing is strong. A novel approach, developed by Hurley (1994), uses particle dispersion in the vertical direction and puff dispersion in the horizontal, and is incorporated into this version of the model. This permits the more accurate particle representation to be used in the vertical, where discontinuities can be large, and where the puff splitting approach has its limitations, while using the puff representation in the horizontal to limit the number of particles that are required to adequately represent the horizontal distribution.

Although the model can be configured to compute dispersion using three-dimensional puff methods (similar to the previous version) or three-dimensional particle dispersion, only the combination (particle-vertical, puff-horizontal) approach will be described in detail here. See Draxler and Hess (1997) for a complete description of the other options. Regardless of which dispersion approach is selected for a simulation, it is first necessary to compute the atmospheric stability, the corresponding atmospheric mixing, and the rate of pollutant dispersion. Each of these processes will be addressed in sequence.

Stability

There are two ways to estimate the boundary-layer stability. The preferred method is to use the fluxes of heat and momentum provided by the meteorological model, if available. Otherwise the vertical temperature and wind gradients at each grid-point are used to estimate stability. This latter situation may not be ideal if meteorological data aloft are only provided on mandatory surfaces with large distances between levels near the ground. In either situation the friction velocity and temperature are estimated first, from which the Obukhov length is calculated.

When surface fluxes are available from the meteorological model, the friction velocity is computed from the momentum flux and the friction temperature is computed from the sensible heat flux. The Obukhov length L is then computed from the friction values, such that

$$z/L = Z_2\, k\, g\, T_* \,(u_*^2\, T_2)^{-1} \qquad -2 \le z/L \le 10 \qquad ...5$$

and where Z_2 indicates height of the second model level, assumed to be the depth of the surface layer.

When no fluxes are provided by the meteorological model, a typical situation when using older meteorological data archives, z/L is estimated from wind and temperature profiles. The meteorological sounding is used first to compute the bulk Richardson Number,

$$R_b = g\, \Delta\theta\, \Delta z\, \{\theta_{12}\, [(\Delta U)^2 + (\Delta V)^2]\}^{-1} \qquad ...6$$

where Δ indicates a gradient between levels 1-2 and θ_{12} is the layer-average virtual potential temperature. Then the stability parameter z/L is estimated from R_b. This is done by using empirical interpolation formulas fit to Monin-Obukhov profile functions explicitly derived for a surface layer height of 75 m (similar equations have been derived by Launiainen (1995), Choudhury et al. (1986), and Abdella and McFarlane (1996)). The friction velocity and temperature are then given by

$$u_* = k\, z_2\, \Delta U\, (\phi_m\, \Delta z)^{-1}, \qquad ...7$$

$$T_* = k\, z_2\, \Delta\theta\, (\phi_h\, \Delta z)^{-1}, \qquad ...8$$

where k is von Kármán's constant ($k \approx 0.4$), and the stability dependent normalised profiles (f) for heat (h) and momentum (m) are from Beljaars and Holtslag (1991) for a stable surface layer ($0 \le z/L \le 10$), and from Betchov and Yaglom (1971) and Kadar and Perepelkin (1989) in an unstable surface layer ($-2 \le z/L \le 0$).

Horizontal and vertical mixing

First the boundary layer depth (Z_i) is computed at each grid-point. It is assumed to equal the height at which the potential temperature first exceeds the value at the ground by 2K. The temperature profile is analysed from the top down to determine the boundary-layer depth. The top-down approach reduces the influence of shallow stable layers near the ground. In addition, a minimum depth of 250 m is assumed for all hours. The height was chosen to correspond with the minimum height resolution typical of the meteorological input data.

The pollutant vertical mixing coefficient (K_z) is assumed to follow the coefficients for heat. Within the Boundary Layer (BL), vertical mixing coefficients are computed following Troen and Mahrt (1986) and Holtslag and Boville (1993), where

$$K_z = k\, w_h\, z\, (1 - z/Z_i)^2 \qquad ...9$$

and w_h is a function of the Prandtl number, $u*$, ϕ_h, ϕ_m, and the convective velocity scale.

Following Beljaars and Betts (1993), mixing through the inversion layer at $z = Z_i$ during convective conditions is computed based upon the surface flux parameters and the strength of the inversion, where

$$K_z = -C_s\, u*\, T*\, (\partial\theta/\partial z)^{-1} \qquad ...10$$

and $C_s = 0.4$. During stable conditions mixing through the interface is calculated from Eqn 11. Above the BL, pollutant mixing in the remainder of the atmosphere is defined by the vertical diffusivity for heat using mixing length theory where

$$K_z = l^2 |\partial V/\partial z|\, \phi(l/L_o)^{-1} \qquad ...11$$

where l is a Blackadar-type mixing length proportional to height above ground and L_o is the local Obukhov length.

Once the K_z profile has been computed, a single average value for the entire BL is computed from the profile and that value replaces all the values within the BL. Each horizontal grid-point will have a different value. The resulting mixing profile, an adaptation of the Troen-Mahrt profiles, was determined empirically to give improved results in both the near and far fields. Although near-field concentrations depend more on the details of the mixing profile while the far-field results depend more upon the average mixing over the BL, the model is intended to be applied for long-range simulations, suggesting a unified approach in averaging the BL mixing.

The subgrid-scale horizontal mixing coefficient (K_h) is computed from the velocity deformation (Smagorinsky 1963; Deardorff 1973),

$$K_h = 2^{-0.5}\, (c\, X)^2\, |\partial U/\partial y + \partial V/\partial x| \qquad ...12$$

where X is the meteorological data grid size, and c is 0.14. Grid scale dispersion is simulated by the particles and puffs horizontally spreading into different wind regimes.

Particle and puff dispersion

Both the horizontal puff and vertical particle dispersion equations are formulated in terms of the turbulent velocity components. These velocity components are a function of the diffusivities computed in the previous section. In the particle model, the dispersion process is represented by adding a turbulent component to the mean velocity obtained from the meteorological data. The approach used follows the one described by Fay et al. (1995) such that after computation of the new position at a time step due to the mean advection of the wind, a turbulent component is added to the mean particle positions (Z),

$$Z_{final}(t+\Delta t) = Z_{mean}(t+\Delta t) + W'(t+\Delta t)\, \Delta t \qquad ...13$$

The contribution of the vertical turbulent wind component (W') is added to the 'mean' position (from Eqn 4) to give a final position from which the advection at the next time step is computed. Full reflection is assumed for particles that intersect the ground or model-top.

The turbulent velocity component at the current time $W'(t+\Delta t)$ is computed from the turbulent velocity component at the previous time $W'(t)$, an autocorrelation coefficient (R) that depends upon the exponential of the time step ($\exp[-\Delta t / T_{Lw}]$), the Lagrangian time-scale (T_{Lw}), and a computer-generated random component (W''), such that

$$W'(t+\Delta t) = R(\Delta t)\, W'(t) + W''\, (1-R(\Delta t)^2)^{0.5} + T_{Lw}\, (1-R(\Delta t))\, \partial\sigma_w^2/\partial z \qquad ...14$$

The last term is applied to prevent accumulation of particles in low turbulence regions (Legg and Raupach 1982), the importance of which is somewhat reduced due to the averaging of the diffusivity profile within the BL. The Lagrangian time-scale is assumed to be a constant 100 s for convenience. This value results in a random walk ($R \approx 0$) vertical dispersion for most of the longer time steps. The random component W'' is the product of a computer-generated Gaussian random number and the standard deviation of the turbulent velocity,

$$\sigma_w = (K_z / T_{Lw})^{0.5} \qquad ...15$$

which is computed from the previously calculated vertical diffusivity (Eqns 9-11).

Puff dispersion is treated in two domains, when the puff is smaller than the meteorological model grid size and when it is larger. In the latter case it is assumed that the meteorological model is capable of resolving turbulent motions on that scale. Gaussian and top-hat' puffs are treated almost identically. When puffs have dimensions less than the meteorological grid spacing, the rate of puff horizontal growth,

$$d\sigma_h/dt = \sqrt{2}\ \sigma_u, \qquad ...16$$

where the horizontal turbulent velocity variance (σ_u) is computed using an equation comparable to Eqn 15 but with the Lagrangian time-scale equal to 10800 s (~1/f) and the diffusivity is from Eqn 12. Additional growth is achieved through the puff-splitting process as the puff grows into different mixing regions. When a puff expands to cover several meteorological grid-points, a top-hat puff splits horizontally into four puffs, each with 25 per cent of the mass, while a large Gaussian puff splits into five smaller puffs, with an additional puff at the centre position with 60 per cent of the mass while the outside four puffs each get 10 per cent of the mass.

Pollutant air concentration

For each puff, concentrations are summed at each time step to all grid-points that fall within the puff defined for top-hat distributions as $\pm 1.54\ \sigma_h$ or $\pm 3.0\ \sigma_h$ for Gaussian distributions. The incremental concentration contribution by each top-hat puff of mass m to a grid-point is,

$$\Delta c = m\,(\pi\ r^2\ \Delta z)^{-1} \qquad ...17$$

where the horizontal radius $r = 1.54\ \sigma_h$. All grid-nodes within the puff receive the same Δc. The incremental concentration contribution for a Gaussian puff is,

$$\Delta c = m\ (2\ \pi\ \sigma_h^2\ \Delta z)^{-1}\ \exp(-0.5\ x^2/\sigma_h^2) \qquad ...18$$

where x is the distance from the puff centre to grid-node and with Δz defined as grid-cell height. Note that, in the vertical, particle calculations are summed into a grid-cell rather than computed at a grid-point. A cell is defined at the centre of the node and has an area corresponding to the half-way distance to adjacent nodes. The final average concentration is the incremental sum divided by the number of time steps in the concentration averaging period.

Air concentration example - ANATEX

Inert atmospheric tracers provide excellent benchmarks for testing atmospheric dispersion models. Most long-range experiments have been conducted under very controlled conditions (pre-selected meteorological conditions), leading to the question of how this practice might be biasing the statistical evaluation of the dispersion models. This problem was addressed in the Across North America Tracer Experiment (ANATEX - Draxler et al. 1991) in which two different inert perfluorocyclohexane gases (PTCH and oc-PDCH) were released for three hours from two different locations, Glasgow, Montana (GGW, 48.4N, 106.5W) and St Cloud, Minnesota (STC, 45.6N, 94.2W) every 2.5 days with about 75 samplers located at weather stations over the whole eastern half of the US. The experiment lasted three months, from 5 January through 29 March 1987.

Dispersion model calculations were made using a consecutive series of forecast (2 to 12 h) meteorological data fields from NOAA's Nested Grid Model (NGM - Peterson and Stackpole 1989) with output fields available every 2 h on a 90 km grid on the NGM's sigma coordinate system (levels at: 0.982, 0.943, 0.897, 0.844, ...). The lowest NGM data level is above the first two dispersion model levels, however the NGM archive contains both heat and momentum fluxes, which were used in the calculation of vertical mixing.

The HYSPLIT model was run for each dispersion combination independently for each source location. The first half of the experimental period was selected for analysis. The model was configured to run for 814 hours, starting with the first release on the 5th of January and ending on the 8th of February. This period includes 14 tracer releases from each location. Only simple statistical analyses were performed on the results. The daily measured and calculated concentrations at each sampling station were averaged over the duration of the simulation. The resulting correlation coefficient was computed from these pairs of measured and model calculated concentrations and it represents the average spatial correlation. The model simulation results are summarised in Table 1.

Table 1. Model performance during ANATEX for the period of 5 January 1987 through 8 February 1987 in terms of the spatial correlation coefficient (R) and the ratio of the mean calculated to mean measured concentrations (C/M). Total computational time is indicated in the last column.

Dispersion Model	*GGW*		*STC*		
Horizontal / Vertical	*R*	*C/M*	*R*	*C/M*	*CPU(h)*
T/T	0.76	1.57	0.55	1.75	1.2
G/T	0.74	1.48	0.56	1.69	2.7
P/P	0.70	1.23	0.65	1.94	2.1
T/P	0.72	1.25	0.69	1.87	2.9
G/P	0.73	1.20	0.72	1.89	6.0

T - top hat puff, G - Gaussian puff, P - Particle dispersion model
CPU - IBM RS6000/590.

In general all model combinations show similar results with a slight over-calculation, higher at STC than at GGW. The three-dimensional puff combinations, T/T and G/T, comparable to the previous version of the model, show correlations that are lower at STC as compared with GGW. Gaussian and top-hat simulations produce almost identical results, with the exception that the Gaussian calculation requires substantially more computer time. The fully 3D particle combination (P/P) or the mixed puff-particle simulations (T/P and G/P) show more comparable results. This is believed to be due to the fact that the STC release was in the middle of the sampling network, and hence there were many more samplers relatively (compared with GGW) close to the release point and hence the statistical results give greater weight to the over-calculation of the nearby samplers. An illustration of the over-calculation can be seen for the T/P combination for GGW in Fig. 4 for both measured and calculated concentrations. The units are 10^{-12} g m^{-3} and the contours are drawn at levels of 10, 20, 50, 100, and 200 units. The basic over-calculation is evident from the larger areal coverage of the calculated contours as compared with the measured contours, especially for the samplers nearest to the release. Because this is a winter period, the strongly stable structure of the atmosphere should increase the model's sensitivity to the vertical mixing computation method. In contrast, if the BL were well mixed, it would matter little if the model mixed pollutants twice as fast or slow as it should at the long source to receptor distances typical of the ANATEX experiment.

One issue regarding the model's sensitivity to the mixing can be addressed by turning on or off various elements of the mixing parametrisation. This test can only be done using the 3D particle version of the model, as it is not possible to compute a concentration at a sampling node for a puff that has no horizontal or vertical dimensions. The results are summarised in Table 2 and it is quite striking that the P/P-2 calculation, where the horizontal equivalent of Eqn 14 equals zero, gives almost identical results to the base simulation (P/P) which included both horizontal and vertical turbulence. Although horizontal dispersion is not explicitly included in the P/P-2 calculation, the vertical mixing of particles into regions of different wind speed and direction results in a horizontal dispersion of particles that dominates the subgrid-scale dispersion parametrisation. The no dispersion (P/P-1) control case and the horizontal dispersion only (P/P-3) simulation show substantial over calculation of air concentration.

Considering the importance of the vertical mixing to the model's performance there are several other simple tests that can be conducted. Varying the Lagrangian time-scale by a factor of two above (T/P-2) and below (T/P-1) the base value of 100s results in concentration changes of greater than a factor of 2 as shown in Table 3. Although the use of the actual K_z profile in the BL (T/P-3) resulted in less overall model bias (more of the tracer remained above the ground), the correlation was less at STC than for the base case (T/P). In the final simulation (T/P-4), z/L was computed from the bulk Richardson number (Eqn 6) rather than defined from the heat and momentum fluxes of the meteorological model and those results were quite comparable to the base case. This result may not hold true for other meteorological data with coarser vertical resolution.

Table 2. Model sensitivity during ANATEX to horizontal and vertical dispersion for the three-dimensional particle version of the model. Statistical measures are as defined in Table 1.

		GGW		*STC*	
Model	*Simulation*	*R*	*C/M*	*R*	*C/M*
P/P	Base - Table 1	0.70	1.23	0.65	1.94
P/P-1	No dispersion	0.36	67.	0.54	108.
P/P-2	Vertical only	0.71	1.22	0.64	1.81
P/P-3	Horizontal only	0.40	53.	0.60	128.

Table 3. Model sensitivity during ANATEX to various vertical dispersion parametrisations for the horizontal-puff, vertical-particle version of the model. Statistical measures are as defined in Table 1.

		GGW		*STC*	
Model	*Simulation*	*R*	*C/M*	*R*	*C/M*
T/P	Base - Table 1	0.72	1.25	0.69	1.87
T/P-1	TLv=50s	0.68	0.51	0.71	0.80
T/P-2	TLv=200s	0.74	2.55	0.65	3.65
T/P-3	No Kz averaging	0.69	0.95	0.57	1.24
T/P-4	No flux fields used	0.71	1.06	0.62	1.76

The last issue regarding the model's vertical structure relates to the computation of the vertical motion. The base calculation uses the vertical velocity field provided in the NGM data fields. However, when the air concentration predictions are recalculated using each of the vertical motion options given by Eqn 2, the results as shown in Table 4 indicate that the isentropic option (T/P-5) provides some improvement in both correlation and bias for both release sites. The same is true, but to a lesser extent, for the isobaric (T/P-6) and isopycnic

(T/P-8) options. However the isosigma calculation (T/P-7) shows a clear and substantial degradation in the results. One can speculate that in a winter stable environment, pollutants are more likely to follow isentropic surfaces, while the terrain-following sigma might be more appropriate during convective conditions when the BL structure is more controlled by the fluxes of heat and momentum from the surface.

Table 4. Model sensitivity during ANATEX to various vertical motion options (Eqn 2) for the horizontal-puff, vertical-particle version of the model. Statistical measures are as defined in Table 1.

		GGW		STC	
Model	*Simulation*	*R*	*C/M*	*R*	*C/M*
T/P	Base - Table 1	0.72	1.25	0.69	1.87
T/P-5	Isentropic	0.78	1.13	0.72	1.65
T/P-6	Isobaric	0.74	0.92	0.71	1.57
T/P-7	Isosigma	0.66	0.84	0.42	2.26
T/P-8	Isopycnic	0.75	0.90	0.70	1.57

Deposition

There are three different removal mechanisms available: dry deposition, wet depletion and radioactive decay. Dry deposition can be either explicitly defined by a deposition velocity, a gravitational settling velocity for particles, or it may be computed using the resistance method. Wet removal for soluble gases is computed from its Henry's Law constant and particle wet removal is computed from a scavenging ratio (l/l) within the cloud and by an explicit scavenging coefficient (s^{-1}) for pollutants below the cloud base. For computational simplicity, the total deposition from both dry and wet removal processes is expressed in terms of inverse time constants which can be added and hence the total deposition over a time step becomes

$$D_{wet+dry} = m \{1\text{-}\exp[-\Delta t (\beta_{dry}+\beta_{gas}+\beta_{inc}+\beta_{bel})]\} \quad ...19$$

where m is the pollutant mass of either the particle or puff. The pollutant mass is then reduced by the deposition amount. Each of the constants, for dry deposition (β_{dry}), wet removal for gases (β_{gas}), in-cloud wet removal of particles (β_{inc}), and below-cloud wet removal of particles (β_{bel}), will be discussed in more detail in the following sections.

Dry removal

Dry removal is computed only when the bottom of the puff or the particle centre position is within the surface layer, defined as the model's second meteorological data level (usually around 75 m). Then the mass deposited by dry removal simply equals the product of the deposition velocity (V_d) and the air concentration, assumed to be uniform over the depth of the pollutant layer (ΔZ_p - in this case the surface layer). The deposition velocity is converted to a removal constant,

$$\beta_{dry} = V_d \, \Delta Z_p^{-1} \quad ...20$$

Figure 4. Average measured and calculated concentrations using the top-hat/particle model combination for the period of 5 January through 8 February, 1987 for tracer releases from the Glasgow, Montana location. Concentration units are 10^{-12} g m^{-3} and the contours are drawn at levels of 10, 20, 50, 100, and 200 units. Values less than 10 approach the detection limit of the analytical system.

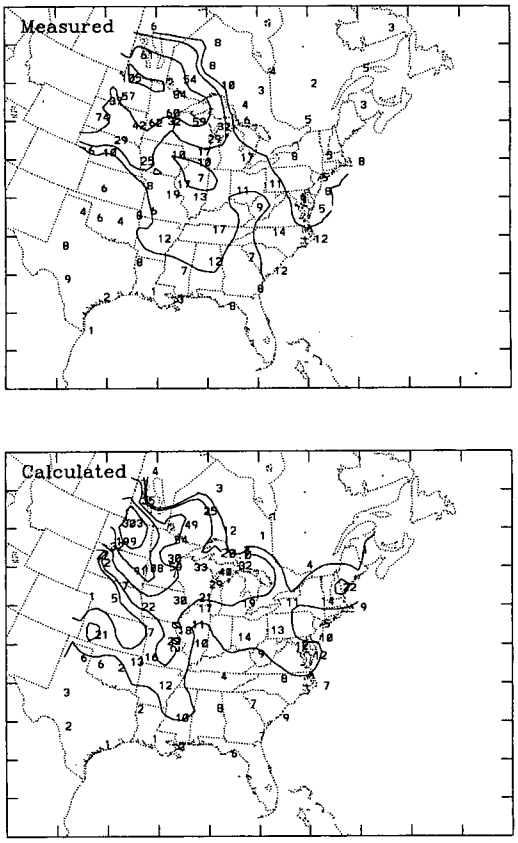

The deposition velocity may be directly specified in the model's input or calculated as the gravitational settling velocity. Particle settling is computed following Van der Hoven (1968) from the particle diameter, air density and particle density. In addition to the resulting mass depletion, the settling velocity is also applied to the pollutant's vertical position each time step to permit the gradual sinking of particles and (non-gaseous) puffs.

The dry deposition velocity may also be computed through the resistance method. Rather than explicitly defining a dry deposition velocity for a pollutant, the total deposition velocity can alternately be computed from the sum of various resistances (Hicks 1986) and the settling velocity for particles such that the total deposition velocity

$$V_d = [\, R_a + R_b + R_c + R_a R_b V_g \,]^{-1} + V_g \qquad ...21$$

where the subscripts for the resistances R, represent the atmospheric layer (a), the quasi-laminar sub-layer (b), and the canopy layer (c) which represents the bulk resistance of various surfaces. Gravitational settling, V_g, is zero for gases and R_c is zero for particles. The resistance components depend upon meteorological conditions as well as the properties of the surface. More detail on each of the resistance components can be found in Draxler and Hess (1997), however, the method very closely follows that proposed by Wesely (1989) as incorporated into the RADM model (Chang 1990), and updated by Walmsley and Wesely (1996).

Wet removal

Wet deposition is divided into two processes (Hicks 1986), those in which the polluted air is continuously ingested into a cloud from a polluted boundary layer and those in which rain falls through a polluted layer. The dominant process is difficult to determine during a model simulation using only the data available from most meteorological archives. Therefore, for particulate pollutants, the simplifying assumption of a scavenging ratio is assumed for pollutants located within a cloud layer and the scavenging coefficient is used for pollutant removal in rain below a cloud layer. The scavenging ratio, which is the ratio of the pollutant's concentration in water to its concentration in air, is expressed as the removal constant,

$$\beta_{inc} = F^t \; F_b \; S \; P \; \Delta Zp^{-1} \qquad ...22$$

where the average scavenging ratio is S=3.2x10^5 by volume, P is the precipitation rate, ΔZp is the depth of the pollutant layer, and F^t is the fraction of the pollutant layer that is below the cloud top. The cloud bottom is defined at the level when the RH first reaches 80 per cent and the cloud top is reached when the RH drops below 60 per cent. Below-cloud removal is defined directly from the value of an average rate constant given by:

$$\beta_{bel} = 5\text{x}10^{-5} \; (1.0\text{-}F_b), \qquad ...23$$

where F_b is the fraction of the pollutant layer that is above the cloud bottom.

The wet deposition of gases depends upon their solubility and for inert non-reactive gases it is a function of the Henry's Law constant (H), the ratio of the pollutant's equilibrium concentration in water to that in air and therefore

$$\beta_{gas} = F^t \; H \; R \; T \; P \; \Delta Zp^{-1} \qquad ...24$$

where R is the universal gas constant, and T is temperature. The wet removal of gases is applied at all levels from the ground to the top of the cloud-layer.

Deposition example – Chernobyl

A good way to illustrate the model's applicability to emergency response situations and evaluate the deposition algorithms is to simulate the situation for the accident at Chernobyl (April 1986). Special meteorological datasets are available from ECMWF (1995) for the accident period. A single 120 h forecast data file, output at 1.125° horizontal resolution every 6 h, was selected for the dispersion simulation, primarily because it contained precipitation fields, not available in the longer time period (12 day) analysis archive. The ECMWF fields have similar vertical resolution as the NGM, but contain additional fields of winds and temperatures, at 10 m and 2 m, respectively. Flux fields were not available and vertical mixing was derived from the wind and temperature profiles.

HYSPLIT was run assuming an emission rate of 10^{15} Bq h^{-1} of Cs-137 for the first 24 h, distributed uniformly in the layer 750-1500 m AGL. Using the default model parameters, i. e., an explicit dry deposition velocity of 0.1 cm s^{-1} (IAEA 1994), a within-cloud scavenging ratio of 3.2 x 10^5 (Hicks 1986), and a below-cloud removal coefficient of 5 x 10^{-5} s^{-1} (Hicks 1986), the model results for Cs-137 deposition are shown in Fig. 5 in units of Bq m^{-2}. The published deposition map (Fig. 6 – from the ATMES report, 1992) for this period shows a deposition peak (at the 50 KBq m^{-2} contour level) over central Sweden while the model predicted a peak of only 18 KBq m^{-2} just to the east over the Baltic Sea. In general, considering that the model is using only forecast precipitation fields and removal constants defined in the literature prior to the accident, the model performance is quite good. Although the radioactive release occurred for a ten-day period, the limited five-day forecast data file only permitted a realistic simulation of the first day's release. The release rate on the

Fig. 5 **The top-hat/particle model simulation of Cs-137 deposition (Bq/m^2) for the first 24 h of emissions of the ten-day Chernobyl accident using the 120 h meteorological forecast from the ECMWF. The concentration grid resolution was 0.5 degrees and the deposition was accumulated from 27 April. Latitude and longitudes are indicated at 10 degree intervals.**

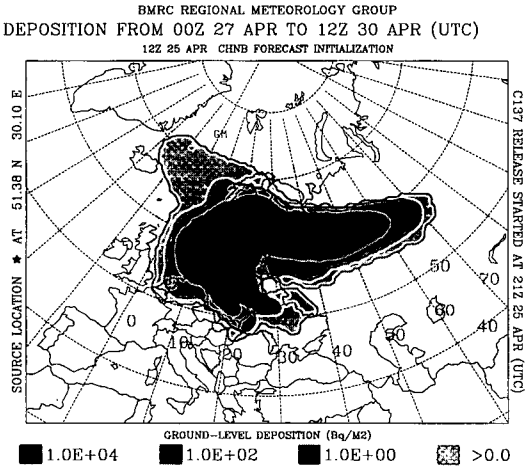

Fig. 6 **Reproduction of the Cs-137 deposition map from the ATMES (1992) report. Includes accumulations from 27 April through 10 May 1986 in units of K Bq/m^2.**

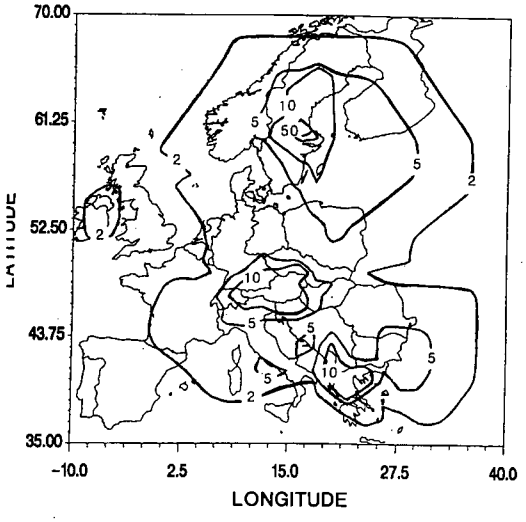

second day dropped to 25 per cent of the rate on the first day, and due to changing meteorological conditions, 90 per cent of the deposition over the Scandinavian countries can be accounted for by the emissions that occurred on the first day. Deposition peaks over central and south-eastern Europe (see Fig. 6) require the simulation to span the duration of the accident.

The sensitivity of some of the assumptions affecting deposition can be evaluated by turning on or off each of the appropriate parameters, the results of which are summarised in Table 5. The default simulation was made using the same model configuration as in all the previous simulations: the horizontal top-hat puff and vertical particle model (T/P). However the same simulation using the puff assumption in the vertical as well as horizontal (T/T) had the greatest effect on the deposition amount, raising the peak to over 50 KBq m^{-2}, an amount almost identical to what was measured. Deposition amounts are higher using the T/T variation of the model because the corresponding air concentrations are higher. Air concentrations are higher using the vertical puff model because by the time the pollutant reached Scandinavia it had mixed up to 3000 m in the particle model but only to 1500 m in the puff model. Measurements in that region (Puhakka et al. 1990) indicated a wide spatial variation in the vertical mixing of the radionuclides, but typical values ranged from 1000 to over 2000 m, indicating that perhaps the vertical puff approximation provided better results in this case, perhaps due to problems in defining an appropriate mixed layer during convective precipitation conditions. The puff representation effectively restrains pollutants within the mixed layer while the particle model will permit a certain fraction to mix through the interfacial layer, the strength of which is defined by Eqn 10.

Table 5. Model computed deposition peaks over the Baltic Sea for the Chernobyl accident using different dispersion and deposition options.

Simulation	*Description*	*Deposition (K Bq m^{-2})*
T/P	Horizontal top-hat/vertical particle	17.7
T/T	Horizontal top-hat/vertical top-hat	55.8
T/P-9	Wet only, no dry (β_{dry}=0)	18.2
T/P-10	Dry only, no wet (β_{inc}=βbel=0)	8.1
T/P-11	In-cloud wet only (β_{bel}= β_{dry}=0)	22.7
T/P-12	Below-cloud wet only (β_{inc}=β_{dry}=0)	3.6
T/P-13	Double in-cloud wet (β_{bel}=β_{dry}=0)	27.0
T/P-14	Half in-cloud wet (β_{bel}=β_{dry}=0)	17.5

Other tests showed that dry removal accounted for about one third of the deposition (T/P-10). However, when dry deposition was turned off and only wet only removal

computed (T/P-9), the maximum deposition was actually greater than in the base case, when both wet and dry removal were turned on (T/P). This result is not inconsistent, in that dry deposition is a continuous process, while wet removal is a function of the spatial and temporal rainfall pattern. Turning off dry deposition permits more material to be transported to the rainfall region where it is subsequently deposited.

One significant feature of the wet deposition computation is that this case is dominated by the in-cloud removal processes (T/P-11 versus T/P-12), accounting for almost all of the wet removal. However increasing (T/P-13) or decreasing (T/P-14) the in-cloud removal coefficient by a factor of two only had a 20 per cent effect on the deposition amount, suggesting that more complicated schemes to determine the removal coefficients will have little effect on the final results and that wet removal is dominated by the rainfall prediction and the vertical distribution of the pollutant.

Volcanic eruptions

All the previous simulations were confined to the lower troposphere, primarily the BL. However a frequently more common application of atmospheric dispersion models, especially as related to emergency response situations deals with the forecasting of the movement of debris from volcanic eruptions, which may penetrate well into the stratosphere. Recent developments in aircraft engine design have made them more sensitive to the effects of volcanic ash. Volcanic eruptions occur much more frequently than nuclear accidents and also provide an opportunity for verification of model performance (Potts 1993).

HYSPLIT required no special modification to handle these kind of events. In the volcanic ash simulation, an emission point would be represented by several particles or puffs, each corresponding to a different size range of ash. The puffs representing each range need to be treated independently because they will have different atmospheric transport pathways due to gravitational settling. The sizes range from diameters of 0.3 to 30 μm, but they all have the same density (2.5 g cm^{-3}), typical of a mix of pumice, basalt and similar materials. This follows the approach developed by Heffter and Stunder (1993) from examination of particle distributions measured after several eruptions in the USA. The release amount for each size range is adjusted according to what fraction of the total mass is represented by that size in the particle distribution. Most of the mass (99 per cent) resides in the 3 to 30 μm range, but the larger particles fall quickly, and only the smallest particles are subject to long-range transport.

The simulation is treated in a manner similar to any point source except that the source is defined at two different heights. The model will then uniformly distribute the pollution between these levels, effectively simulating a vertical line source from an explosive eruption. The Rabaul eruption of 2000 UTC 18 September 1994 was selected for the example simulation. A continuous release (1 unit h^{-1}) between 1000 m to 22000 m AGL was used to represent the eruption. The simulation, using the 381 km NOAA final analysis data, was run for only five hours and the output, shown on Fig. 7, represents the instantaneous concentration at 0030 UTC 19 September. This is the time of the GMS VIS satellite photograph shown in Fig. 8. The bulk of the ash is at the upper levels and the correspondence, in terms of the extent and shape of the cloud, is quite good. Although the southern edge of the visible cloud is not bright, it extends to nearly 7°S. On the corresponding lower resolution IR image (not shown) some material appears west of 150°E and north of 4°S; these features are present on the VIS image but are diffuse. There is some uncertainty about the eruption height, as is the case in most of these events, assumed to be constant from the start of the release to the time of the satellite photo. Stereo conical scans using other satellites showed considerable height variations over the cloud domain. Although the satellite verification shown here is rather qualitative, it does demonstrate that the same model can be effectively applied to a variety of different air quality simulations.

Fig. 7 Simulation of the Rabaul volcanic eruption of 2000 UTC 18 September 1994 showing the vertical column-averaged snapshot air concentrations at 0030 UTC 19 September 1994. Concentrations are only qualitative as the eruption mass was unknown. The concentration grid resolution was 0.1 degrees. Latitude and longitudes are indicated at 2 degree intervals.

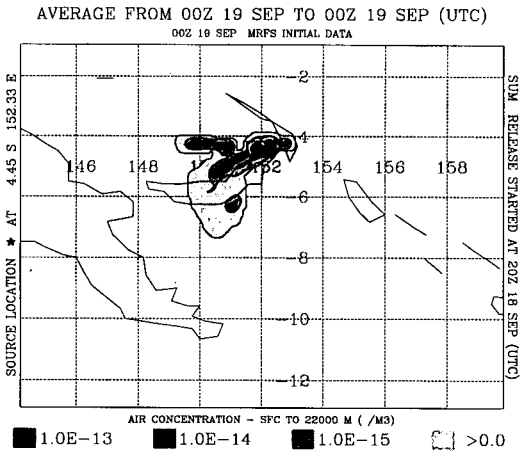

Fig. 8 **GMS VIS satellite photo for 0032 UTC 19 September 1994, a time that corresponds to the time of the simulation shown in Fig. 7.**

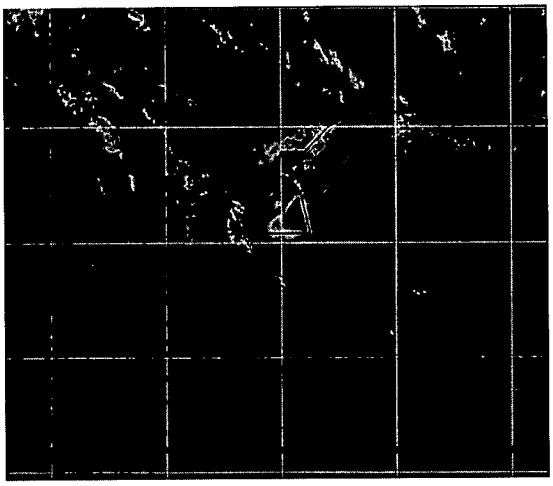

Summary

A description, overview of the equations, and example calculations from HYSPLIT_4, a Lagrangian model that can be used to calculate trajectories and air concentrations for analytical studies and to support atmospheric emergency response applications, has been presented. The configuration of the model was shown to be generic in that it could be set up to perform a variety of different scenarios. In general, Lagrangian models are well suited for quick calculations from pollutant point sources and such a modelling approach is ideal for situations where quick turnaround is essential; i.e., about 1 to 3 min CPU time per simulation day. The model's performance has been evaluated in a qualitative sense by comparing the calculations for a variety of different applications to real data observations, such as measured balloon trajectories, measured air concentrations of inert tracers, measured radioactive deposition, and satellite photographs of ash from volcanic eruptions. In general the model's performance compared favourably to the observations in all areas, although there is still room for improvement, with particular regard to the vertical distribution of pollutants in different meteorological regimes. The model's performance has been found to be sensitive to the low-level wind profile (for BL trajectories), the vertical mixing coefficients (for air concentrations), and the interaction of the vertical pollutant distribution and the rainfall field (for deposition). Clearly all aspects of model performance were related to how well the vertical atmospheric structure is reproduced, either in the meteorological fields of the input data driving the calculations, or in the parametrisations used to estimate pollutant vertical mixing. Clearly this continues to be an active area of research and our computational methods will be modified accordingly.

Acknowledgments

The authors would like to thank Steve Businger, University of Hawaii, for providing the ACE balloon observations; Steve Siems, Monash University, Clayton, Victoria, for the ACE trajectory calculations using the GASP data; Fred Prata, Division of Atmospheric Research, CSIRO, Aspendale, Victoria, for providing rather unique insights to the details about the Rabaul volcanic eruption; Gang Liang, BMRC, for development of the HYSPLIT graphical user interface; Les Logan, BMRC, for developing some of the NCAR graphics display routines and an interface for the BoM meteorological data; and David Pike, BMRC, for the preparation of graphics and satellite photographs.

References

Abdella, K. and McFarlane, N.A. 1996. Parametrisation of the surface-layer exchange coefficients for atmospheric models. *Bound. Lay. Met., 80,* 233-48.

ATMES Report. 1992. *Evaluation of long range atmospheric transport models using environmental radioactivity data from the Chernobyl accident.* W. Klug, G. Graziani, G. Grippa, D. Pierce, and C. Tassone (Eds), Elsevier Science Publishers, Linton Rd., Essex, England.

Bates, T.S., Huebert, B.J., Gras, J.L., Griffiths, F.B. and Durkee, P.A. 1998. International global atmospheric chemistry (IGAC) project's first aerosol characterization experiment (ACE 1): Overview. *J. geophys. Res., 103,* 16297-318.

Beljaars, A.C.M. and Betts, A.K. 1993. *Validation of the boundary layer representation in the ECMWF model.* Proc. of a Seminar Held at ECMWF on Validation of Models over Europe, Vol. II, 7-11 September, 1992, European Centre for Medium-Range Weather Forecasts, Shinfield Park, UK, 159-95.

Beljaars, A.C.M. and Holtslag, A.A.M. 1991. Flux parametrisations over land surfaces for atmospheric models. *Jnl appl. Met., 30,* 327-41.

Betchov, R. and Yaglom, A.M. 1971. Comments on the theory of similarity as applied to turbulence in an unstably stratified fluid. *Atmos. Oceanic Phys., 7,* 82932.

Bourke, W., Hart, T., Steinle, P., Seaman, R., Embery, G., Naughton, M. and Rikus, L. 1995. Evolution of the Bureau of Meteorology global assimilation and prediction system. Part 2: Resolution enhancements and case studies. *Aust. Met. Mag., 44,* 19-40.

Chang, J.S. 1990. Appendix E, NAPAP Report 4, The regional acid deposition model and engineering model, in Acid Deposition: *State of Science and Technology, Vol I,* Emissions, Atmospheric Processes, and Deposition, U.S. Government Printing Office, Washington D.C., 20402-9325.

Choudhury, B. J., Reginato, R. J. and Idso, S. B. 1986. An analysis of infrared temperature observations over wheat and calculation of latent heat flux. *Agric. Forest Meteor., 37,* 75-88.

Deardorff, J.W. 1973. Three-dimensional numerical modelling of the planetary boundary layer. *Workshop on Micrometeorology,* D.A. Haugen, Ed., American Meteorological Society, 45 Beacon St., Boston, MA, 02108, 271-311.

Draxler, R.R. 1990. The calculation of low-level winds from the archived data of a regional primitive equation model. *Jnl appl. Met., 29*, 240-8.

Draxler, R.R. 1991. The accuracy of trajectories during ANATEX calculated using dynamic model analyses versus rawinsonde observations. *Jnl appl. Met., 30*, 1446-67.

Draxler, R.R. 1992. Hybrid single-particle Lagrangian integrated trajectories (HY-SPLIT): Version 3.0 – User's guide and model description. *NOAA Tech. Memo. ERL ARL-195*, 26 pp. and Appendices. [Available from National Technical Information Service, 5285 Port Royal Road, Springfield, VA 22161.]

Draxler, R.R. 1996. Trajectory optimization for balloon flight planning, *Weath. forecasting, 11*, 111-14.

Draxler, R.R., Dietz, R., Lagomarsino, R.J. and Start, G. 1991. Across North America Tracer Experiment (ANATEX): Sampling and Analysis. *Atmos. Environ., 25A*, 2815-36.

Draxler, R.R. and Hess G.D. 1997. Description of the HSYPLIT_4 modelling system, *NOAA Technical Memorandum ERL ARL-224*, December, 24 pp., [Available from National Technical Information Service, 5285 Port Royal Road, Springfield, VA 22161.]

Draxler, R.R. and Stunder, B.J.B. 1988. Modelling the CAPTEX vertical tracer concentration profiles. *Jnl appl. Met., 27*, 617-25.

Draxler, R.R. and Taylor, A.D. 1982. Horizontal dispersion parameters for long-range transport modelling. *Jnl appl. Met., 21*, 367-72.

ECMWF 1995. *The description of the ECMWF/WCRP level III-A global atmospheric data archive*. European Centre for Medium-Range Weather Forecasts, Reading, Berkshire, England.

Fay, B., Glaab, H., Jacobsen, I. and Schrodin, R. 1995. Evaluation of Eulerian and Lagrangian atmospheric transport models at the Deutscher Wetterdienst using ANATEX surface tracer data. *Atmos. Environ., 29*, 2485-97.

Heffter, J.L. and Stunder, B.J.B. 1993. Volcanic ash forecast transport and dispersion (VAFTAD) Model. *Weath. forecasting, 8*, 533-41.

Hicks, B.B. 1986. Differences in wet and dry particle deposition parameters between North America and Europe. In *Aerosols: Research, Risk Assessment, and Control Strategies*, Lewis Publishers, Chelsea, MI, pp 973-982.

Holtslag, A.A.M. and Boville, B.A. 1993. Local versus nonlocal boundary-layer diffusion in a global climate model. *Jnl climate, 6*, 1825-42.

Hurley, P. 1994. PARTPUFF - A Lagrangian particle-puff approach for plume dispersion modelling applications. *Jnl appl. Met., 33*, 285-94.

IAEA 1994. Modelling the deposition of airborne radionuclides into the urban environment. First report of the VAMP Urban Working Group, International Atomic Energy Agency, *Technical Document 760*.

Kadar, B.A. and Perepelkin, V.G. 1989. Effect of the unstable stratification on wind and temperature profiles in the surface layer. *Atmos. Oceanic Phys., 25*, 583-8.

Kreyszig, E. 1968. *Advanced engineering mathematics*. 2nd Ed. J. Wiley and Sons, New York, 898 p.

Launiainen, J. 1995. Derivation of the relationship between the Obukhov stability parameter and the bulk Richardson number for flux-profile studies. *Bound. Lay. Met., 76*, 165-79.

Legg, B.J. and Raupach, M. 1982. Markov chain simulation of particle dispersion in inhomogeneous flows: the mean drift velocity induced by a gradient in Eulerian velocity variance. *Bound. Lay. Met., 24*, 3-13.

Peterson, R.A. and Stackpole, J.D. 1989. Overview of the NMC production suite. *Weath. forecasting, 4*, 313-22.

Petterssen, S. 1940. *Weather analysis and forecasting*. McGraw-Hill Book Company, New York, 221-3.

Potts, R.J. 1993. Satellite observations of Mt Pinatubo ash clouds. *Aust. Met. Mag., 42*, 59-68.

Puhakka, T., Jylhä, K., Saarikivi, P., Koistinen, J. 1990. Meteorological factors influencing the radioactive deposition in Finland after the Chernobyl accident. *Jnl appl. Met., 29*, 813-29.

Smagorinsky, J. 1963. General circulation experiments with the primitive equations: 1. The basic experiment. *Mon. Weath. Rev., 91*, 99-164.

Taylor, A.D. 1997. Conformal map transformations for meteorological modelers. *Computers and Geosciences, 23*, 63-75.

Troen, I. and Mahrt, L. 1986. A simple model of the atmospheric boundary layer: sensitivity to surface evaporation. *Bound. Lay. Met., 37*, 129-48.

Van der Hoven, I. 1968. Deposition of particles and gases. In *Meteorology and Atomic Energy*, D. Slade (Ed.), TID-24190, NTIS, Springfield, VA, 445p.

Walmsley, J. L. and Wesely, M. L. 1996. Modification of coded parametrizations of surface resistances to gaseous dry deposition. *Atmos. Environ., 30*, 1181-8.

Wesely, M.L. 1989. Parametrisations of surface resistances to gaseous dry deposition in regional-scale numerical models. *Atmos. Environ., 23*, 1293-304.